Charge-density-wave noise propagation in the blue bronzes $Rb_{0.3}MoO_3$ and $K_{0.3}MoO_3$

T. Csiba, G. Kriza, and A. Jánossy
Central Research Institute for Physics, P.O. Box 49, H-1525 Budapest, Hungary
(Received 6 July 1989)

A voltage instability in the charge-density-wave conducting state of $Rb_{0.3}MoO_3$ and $K_{0.3}MoO_3$ is investigated. Voltage pulses are created at a well-defined location within the sample and propagate along the crystal. With increasing field the pulse creation frequency increases, and the pulses merge into a narrow-band oscillation. The field and temperature dependence of characteristic quantities is given. The results are interpreted in the framework of a moving charge-density-wave dislocation model by Lee and Rice. The consequences on the origin of narrow-band voltage noise are also discussed.

I. INTRODUCTION

The understanding of sliding charge-density-wave (CDW) conduction[1] has evolved fast since the first experimental observations in the late 1970s. In 1976 Monceau *et al.*[2] found a nonlinear conductivity in the incommensurate CDW system, $NbSe_3$. Bardeen[3] attributed the observation to conduction by the "sliding" motion of the CDW predicted by Fröhlich[4] more than two decades before. It was not much later that Fleming and Grimes[5] discovered perhaps the most amazing phenomenon of sliding CDW conduction: there is an oscillating component in the voltage response of the system to a dc current.[6] The importance of CDW noise studies is sometimes compared to that of tunneling phenomena in superconductors. There is, however, an important conceptual difference: while the main features of superconducting tunneling had been predicted theoretically, the source of CDW conduction noise is still debated after ten years of intensive research.

The dominant trend in theory is to take only phase excitations into account in CDW dynamics. In zero external field the CDW is pinned by the interaction with various imperfections of the underlying crystal lattice. The CDW phase also couples to an external electric field, and the field depins the CDW at a well-defined threshold,[5] E_T, above which the nonlinear conduction occurs. The CDW conduction noise has a periodic component called narrow-band noise[5] (NBN). In good quality, small-volume $NbSe_3$ samples the quality factor of this oscillation can be as high as 10^4 (Ref. 7), so the term "noise" is somewhat misleading. A broadband noise[5,8] with power spectrum often fitted to $f^{-\alpha}$ coexists with the NBN. Various other instabilities, such as steplike, nonperiodic changes in the voltage[9] or quasiperiodic voltage pulses[10–12] have also been reported. The above noise phenomena are common to all model systems of sliding CDW conduction.

The most remarkable feature of NBN is that its frequency is proportional to the current carried by the CDW.[13] This proportionality has been verified over a wide range of frequencies and currents.[14] Assuming that during one period of the oscillation the CDW is displaced by one wavelength λ, we obtain the following proportionality constant:

$$j_{\mathrm{CDW}}/\nu = n_c e \lambda \ , \tag{1}$$

where j_{CDW} is the CDW current density, ν is the NBN frequency, n_c is the density of condensed electrons, and e is the electronic charge. Equation (1) has been verified[15] on $Rb_{0.3}MoO_3$ with high accuracy, and is also consistent with measurements[16,17] on other model systems of sliding CDW conduction. At low temperatures where n_c saturates, Eq. (1) means that the charge displaced during one period of oscillation is $2e$ per conducting chain.

Several models have been constructed to understand the generation of NBN. In one type of model[18,19] NBN is generated in the bulk of the crystal due to the interaction of the CDW with lattice imperfections. The pinning potential which is the result of the collective effect of pinning centers is periodic with respect to a translation of the CDW by λ. This leads to a periodic modulation of the CDW sliding velocity. Since the velocity-velocity correlation is finite, the voltage oscillations disappear in the thermodynamic limit.

Other models[20–22] assume that the noise originates at the boundaries of pinned and unpinned regions. In the model put forward by Ong, Verma, and Maki[20,21] NBN is generated by dislocations of the CDW superlattice, which are moving perpendicularly to the conducting axis between sliding and pinned regions at electrode contacts. A direct consequence of the local noise generation is that the noise amplitude is constant as the sample length tends to infinity. The results of experiments[20,23–25] aimed to distinguish between local and bulk noise generation by measuring the volume (sample length) dependence of noise amplitude are controversial. Similarly, NBN measurements[20,26–29] on samples with inhomogeneous temperature distribution have been inconclusive.

Although there is no direct experimental evidence of the existence of CDW dislocations in quasi-one-dimensional materials, recent theories[30–33] increasingly recognize their importance in CDW dynamics. It is well documented[15,34] that the CDW current density is usually

inhomogeneous, and the simultaneous destruction of CDW order at the whole surface of the boundary between regions with different sliding velocities is certainly less favorable than the creation of dislocation lines moving on the boundary. Besides NBN, experimental observations attributed to CDW dislocations include the enhancement[35–37] of the threshold electric field in short samples. This enhancement of E_T has been explained[35,37] by a contribution from dislocation creation.

In a recent letter[38] we have reported on a voltage instability appearing at the threshold field for CDW conduction in a $Rb_{0.3}MoO_3$ crystal. We have found that voltage pulses appear with a time delay on consecutive sample segments, i.e., the pulses propagate along the crystal. The propagation velocity is in the order of 1 m/s, orders of magnitude smaller than the phason velocity. The frequency of the pulses increases with increasing electric field, and at high frequencies the pulses from periodic oscillations resembling the NBN.

In this paper we give a detailed characterization of this noise propagation phenomenon based on measurements on several $Rb_{0.3}MoO_3$ and $K_{0.3}MoO_3$ samples. A thorough description of the electric field and temperature dependence of the characteristic quantities such as propagation delay and the charge associated with the pulses is presented. Our data suggest that the extra CDW current associated with the pulses satisfy Eq. (1). We show that the pulses can be synchronized, or "mode locked" to an external ac drive, which is a well-known feature[6,13] of NBN. The pulses are shown to be created at a well-defined location within the sample, and by experiments using intentionally inhomogeneous current distributions we attempt to investigate the pulse creation and pulse propagation separately. We suggest that the origin of the voltage instability may be the same as that of any "narrow-band noise," and local generation and low velocity propagation may be a generic feature of NBN. We interpret our findings in the framework of the moving dislocation loop model by Lee and Rice.[39]

II. EXPERIMENT

A. Techniques

We have investigated $Rb_{0.3}MoO_3$ and $K_{0.3}MoO_3$ "blue bronze" single crystals. These two materials have identical properties for our purposes and both undergo a Peierls distortion at $T_P=180$ K where incommensurate CDW's are formed. All the signatures of sliding CDW conduction have been found and thoroughly investigated[40] in both systems.

The single crystals used in this study have regular rectangular shapes with the dimension corresponding to the CDW sliding direction much larger than the perpendicular ones. Four electroplated copper contacts were applied to the ultrasonically cleaned crystal surfaces. The contacts divide the sample into three consecutive segments labeled *A*, *B*, and *C*. We have studied three $Rb_{0.3}MoO_3$ samples denoted by *RBL*, *RBM*, and *RBN*, and two $K_{0.3}MoO_3$ samples, *KL* and *KM*. The dimensions of a typical sample, *RBL*, on which a considerable part of the data presented here have been measured are 1.5 mm×110 μm×36 μm. The length of a contact is 150–250 μm. The current-voltage (*I-V*) characteristics of sample *RBL* are shown in Fig. 1. The characteristics display a sharp threshold field for nonlinear conduction, $E_T=0.42$ V/cm at 77 K, and a strong nonlinearity above threshold. Similar *I-V* characteristics have been measured on the other crystals.

The sample was driven by a Keithley 220 current source or a Keithley 230 voltage source with an external resistance in series at least 40 times (typically 100 times) larger than the sample resistance to ensure constant current drive. The arrangement is depicted in the inset of Fig. 1. The voltage responses of all the three segments were monitored simultaneously by dc differential amplifiers with an upper cutoff frequency of 10 kHz. The preamplifier output was digitized by a Tektronix 5223 oscilloscope, and transferred to a computer for processing.

Careful checks have been carried out to exclude spurious time delays or crosstalks of the signals of the different segments. By applying a small amplitude 10-kHz ac current to the sample we have verified that the instrumental time delays between segments are smaller than our time resolution of a few microseconds. We have also checked that interchanging the preamplifiers does not affect the measured signals. To estimate the crosstalk between segments we have applied a 1-kHz ac signal to segment *A* (*C*) in addition to the dc current flowing through the sample, and detected on segment *C* (*A*). The crosstalk was small, about −40 dB, the value expected from the known source and load resistances in a linear circuit.

B. Basic characteristics of noise propagation

In this section we first illustrate the basic properties of the noise propagation phenomena by data measured on sample *RBL* at 77 K. Then we describe the temperature variation of the characteristic quantities. Finally a comparison with findings on other samples is given. Sections II C and II D are devoted to the more complex ac-dc interference and inhomogeneous current experiments.

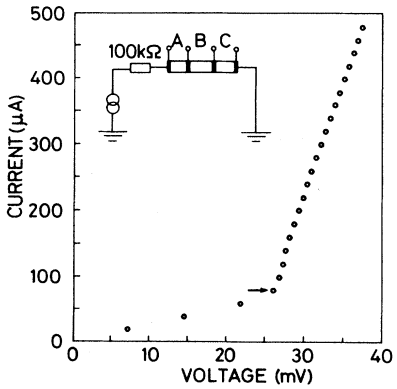

FIG. 1. The current-voltage characteristics of segment *B* of sample *RBL* measured in the configuration shown in the inset. The voltage pulses of Fig. 2 appear at the current indicated by the arrow ($T=77$ K).

Upon increasing the current from below threshold, pulses in the voltage response appear, correlated in all the three segments. Figure 2 shows the evolution of the pulse pattern with increasing current at 77 K. The pulses first appear at a current very close, although significantly above threshold. The amplitude of the pulses is a few hundred microvolts, i.e., 1–2 % of the total voltage. As the current increases, the time separation of the pulses decreases rapidly until they form a continuous train of current oscillations. At even higher currents the quasiperiodic nature of the pulses is lost and a chaotic response appears (not shown in Figure 2). This pattern is very similar to those observed by Gill and Higgs[10] in $NbSe_3$, Ong *et al.* in TaS_3,[12] and by Dumas *et al.* in $K_{0.3}MoO_3$.[11]

To characterize the temporal coherence of successive pulses on a given segment, we have averaged the Fourier power spectra of time records. Three representative spectra are shown in Fig. 3. At low repetition rates the time separation of pulses varies randomly corresponding to a broad frequency spectrum. A well-defined peak appears at higher currents, which narrows with increasing field. The peak is the narrowest at about 100 Hz, then it broadens again. Above 150 Hz the peak disappears, and only a broad shoulder is observed.

Figure 4 shows voltage pulses recorded simultaneously on all three segments. It is obvious from Fig. 4(a) (taken at a low repetition rate) that the same pulse appears on all segments, but with a delay on segment *B*, and with an even larger delay on segment *C*, compared to segment *A*. This sequence of delays proves that the pulses are due to instabilities that *propagate* along the crystal. They are created in segment *A*, and travel towards segment *C*, which corresponds to the direction of negative charge carrier flow. The propagation delay is in the order of 1 ms, corresponding to a propagation velocity of about 1 m/s. The delay is comparable to but smaller than the pulse width. The pulses in Fig. 4(b) were taken at a higher current. Here the propagation delay shows up as a constant phase shift between the oscillations on the different segments.

Because of the low signal-to-noise ratio, we have applied different averaging methods to measure the propagation delay of pulses. In the first method which we have used at low frequencies, we average the oscilloscope traces triggered from the pulse itself in the pretrigger mode of the oscilloscope. We take the time difference of the minima of averaged signals as the propagation delay. The averaged signals are only slightly broader than the single shot ones.

In an alternative method we calculate the cross-

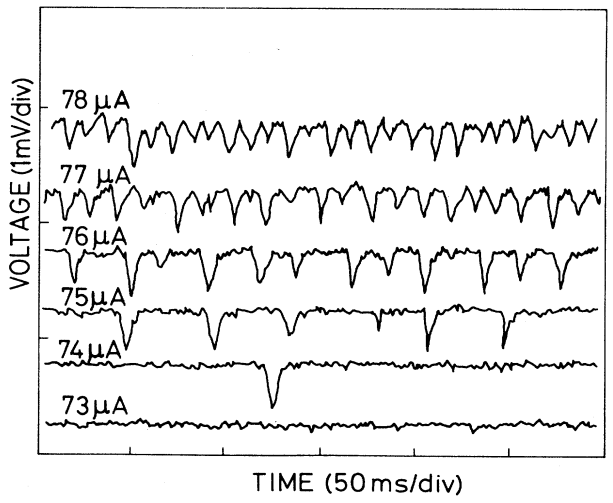

FIG. 2. Voltage response to different dc currents in the vicinity of the nonlinear threshold current. Voltage pulses appear in the response above the threshold (sample *RBL*, $T=77$ K).

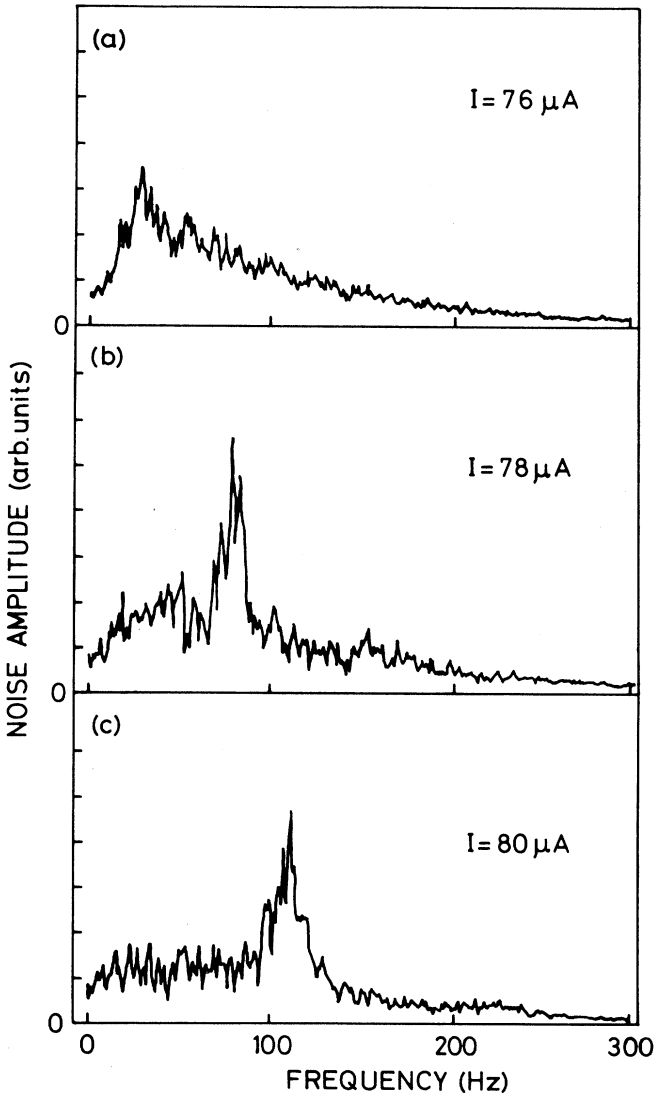

FIG. 3. Fourier amplitude spectra of the CDW voltage noise at different currents. (a) At low currents, i.e., at low-pulse creation frequencies the voltage pulses are aperiodic. (b) At higher currents a sharp peak appears in the spectrum indicating that the pulses form quasiperiodic oscillations with well-defined frequency. (c) The frequency of the peak increases with increasing current (sample *RBL*, $T=77$ K).

correlation function, C_{ij}, of the signals of segments i and j: $C_{ij}(\tau)=(1/t_0)\int \Delta V_i(t)\Delta V_j(t+\tau)dt$, where $\Delta V_i(t) = V_i(t)-(1/t_0)\int V_i(t)dt$ (t_0 is the length of the time record), and average the correlation functions instead of the direct signal. In this case we define the time delay τ_{ij} between segments i and j as the maximum position of C_{ij}. We have used this method at all frequencies.

The two methods gave similar results although τ calculated by the correlation method tended to be slightly higher than that by the direct average method. Figure 5 displays the dependence of the delay τ_{AC} on electric field at $T=77$ K, measured by the correlation method. With increasing field the delay decreases, i.e., the propagation velocity increases. Another representation of the data is shown in the inset of the figure: the delay is plotted against the inverse repetition frequency, $1/f$. The delay seems to saturate at low frequencies, τ remains finite as $1/f\rightarrow\infty$.

The pulses are of very similar shape on all segments, although some broadening can be observed as the pulse travels from A toward C. During the pulse, the voltage first drops sharply and then returns to the baseline more slowly. Averaging over a large number of signals reveals

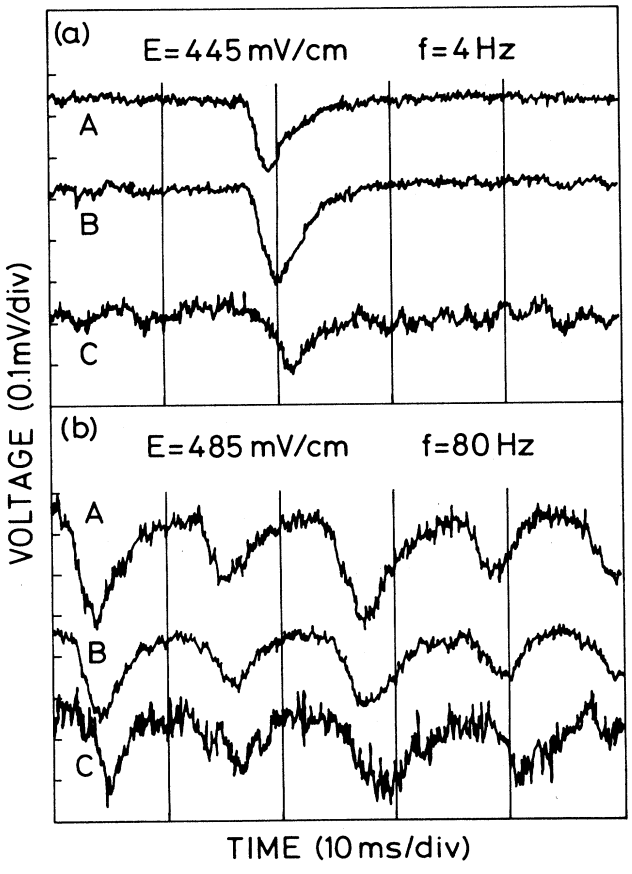

FIG. 4. Voltage pulses recorded simultaneously on the three sample segments A, B, and C (see the inset in Fig. 1). The pulses appear with a time delay on consecutive segments indicating a propagation from A towards C. (a) and (b) were taken at two different currents (sample RBL, $T=77$ K).

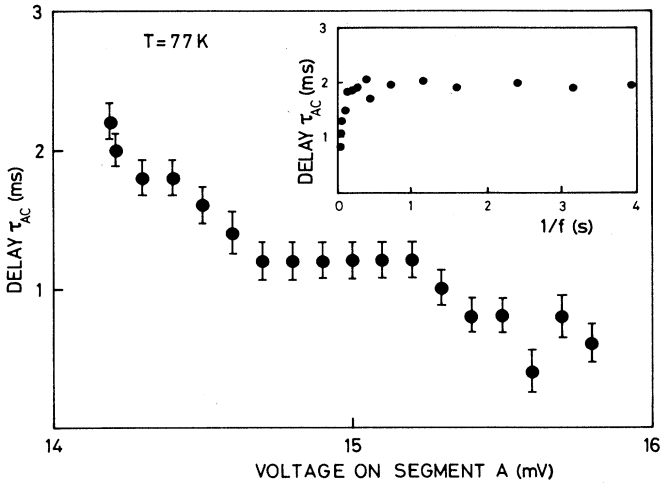

FIG. 5. The time delay, τ_{AC}, between voltage pulses on segments A and C as a function of the dc voltage on segment A. The inset shows τ_{AC} as a function of the inverse repetition frequency of the pulses. The delay remains finite at low repetition frequencies (sample RBL).

a small amplitude tail of the pulse for times as long as 10–100 s, i.e., up to 10^4 times the pulse width at half maximum. While the pulse always corresponds to a conductivity increase, the tail may be both an increase or decrease compared to the state preceding the pulse. The sign of the tail may change from segment to segment. We attribute this very long-time tail to a change in the normal resistance as will be discussed later in more detail.

We approximate the charge carried by the extra CDW current, $I_{\rm CDW}$, associated with a pulse in segment i by

$$Q_i=\int I_{\rm CDW}dt=\frac{1}{R_i}\int \Delta V_i(t)dt\ , \tag{2}$$

where R_i is the resistance of the segment, and ΔV_i is the deviation of the voltage from a "baseline" measured far enough before the pulses. This calculation is carried out only for pulses with wide enough separation where the baseline could be determined. To separate the contribution to the integral of the long-time tail—assumed to have a different origin—the upper bound was chosen to be about five times the pulse width at half maximum. Changing this upper bound by a factor of 2 caused only a few percent change in the calculated charge.

The charge Q_i calculated this way fluctuates from pulse to pulse. Figure 6 shows the distribution of charge magnitudes at two different repetition frequencies obtained at slightly different electric fields. The distributions are structureless, no sign of charge quantization is observed. At the lower frequency the distribution is symmetric and relatively sharp, the width at half maximum is about $\pm 15\%$ of the average charge. With increasing field the distribution broadens and becomes asymmetric: a tail on the low-charge side appears. The maximum of the distribution moves to a higher charge, but the mean value is unchanged within 10%. This field independence of the mean charge has been checked at several fields up to the

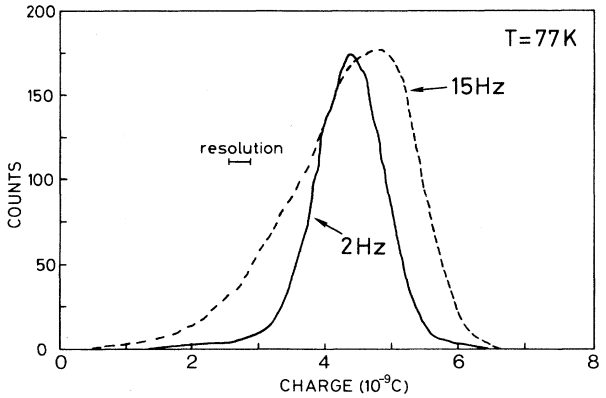

FIG. 6. The distribution of the charge associated with the pulses at two different pulse creation frequencies: $\nu=2$ Hz (solid line) and $\nu=15$ Hz (dashed line). The distributions have been obtained by calculating the area of each of 20 000 pulses and by constructing a histogram of the areas. The areas have been converted to charge using Eq. (2). The histogram has been smoothed, the resolution is indicated in the figure (sample *RBL*, $T=77$ K).

highest frequency where the baseline determination is still possible (about 15 Hz). The Q_i charges associated with the same pulse on different segments are the same within a factor of 2. The average charge is in the order of $2e$ per chain. Using a per chain cross-sectional area of 4.16×10^{-19} m^2, a $2e$ charge per chain is 3×10^{-9} C for sample *RBL*.

The current in the pulses is estimated by $Q\nu$, while the total nonlinear current is determined by dc *I-V* measurements. Since the threshold field for nonlinear conduction is somewhat lower than the threshold field for pulse creation, the fraction of nonlinear current carried by the pulses is very small when the pulses first appear. With increasing field this fraction increases to about 10%.

Figure 7 shows the temperature dependence of the delays between pulses appearing on different segments and of the pulse width at a fixed pulse repetition rate. All these quantities increase with decreasing temperature at a rate close to that of the normal resistance. This observation is in accordance with the general property of CDW systems that the time scales characteristic of CDW dynamics increase exponentially with decreasing temperature. On the other hand the charge Q associated with the pulses does not change with temperature within experimental uncertainly in the temperature range of 60 to 80 K.

The basic features of noise propagation described above for sample *RBL* have been confirmed on other samples. Voltage pulses similar in shape to those in Figs. 2 and 4, appearing with a delay on different segments, have been observed on all crystals investigated. The repetition frequency increases and the delay decreases with increasing electric field.

Figure 8 illustrates the pulse propagation in a $K_{0.3}MoO_3$ sample, *KM*. It is obvious from the figure that not only the pulse minima are delayed on different segments, but also the leading edges of the pulses: when the

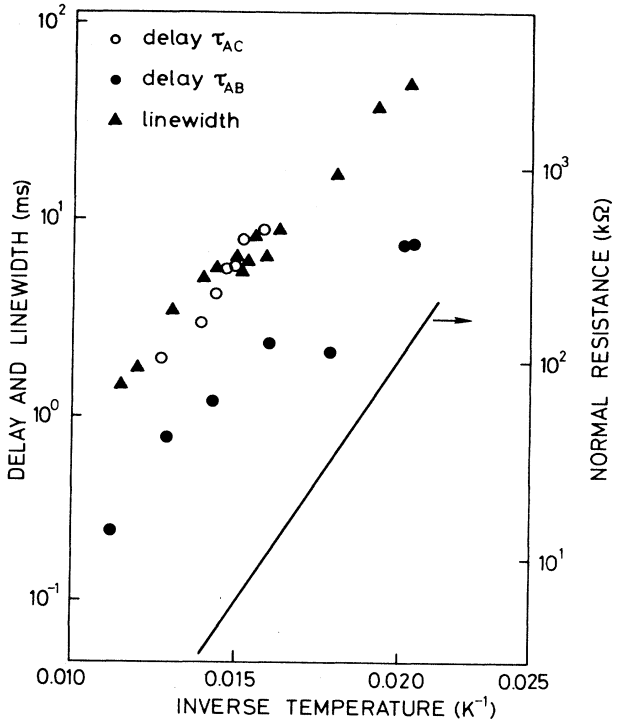

FIG. 7. The linewidth of pulses on segment A, the time delay between the pulses on A and $B(\tau_{AB})$, and between A and $C(\tau_{AC})$ as a function of the inverse temperature. At all temperatures the pulse repetition rate was 10 Hz. The solid line shows the temperature dependence of the normal resistance (sample *RBL*).

voltage on segment A starts to drop significantly below the baseline no deviation from the baseline occurs on segments B and C for a while.

The pulse does not always propagate through all three segments. This feature is illustrated in Fig. 9 where a pulse appears on segments A and B, but does not

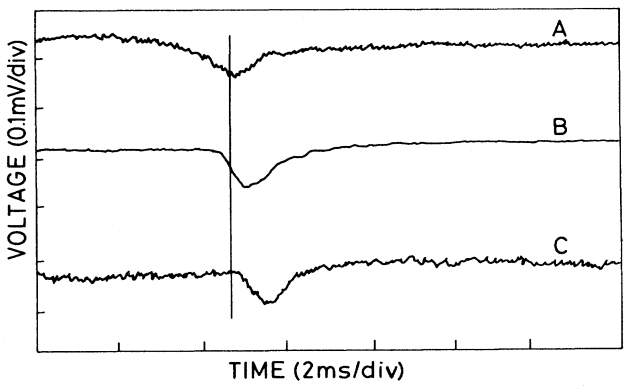

FIG. 8. Time-delayed pulses on the segments of sample *KM*. The curves are averages of 10 oscilloscope traces triggered from the pulses in pretrigger mode. In this sample the ratio of the time delay to the pulse width is high, and the delay of the leading edges of the pulses is well visible. (The vertical line is a guide to the eye.)

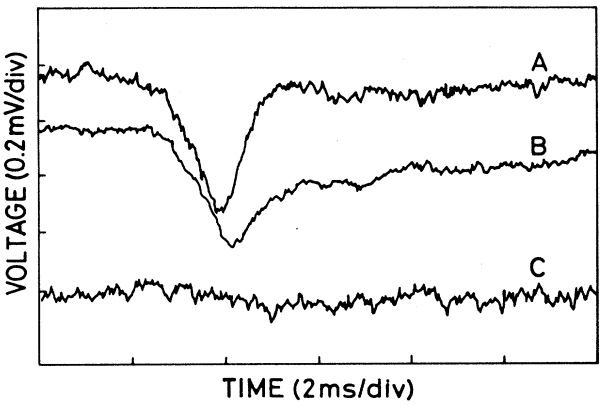

FIG. 9. Pulses in sample *RBM* demonstrate that some pulses appear only on two adjacent segments but not on the third one.

penetrate into segment *C*. However, under the same circumstances, some pulses do appear on all three segments. Figure 9 also confirms directly that the correlated appearance of pulses on different segments is not due to some spurious crosstalk effect. We conclude that the pulses are created at a well-defined source within the crystal, but the location of annihilation may vary from pulse to pulse. In some cases more than one source operates simultaneously. In the following chapter we shall further demonstrate the asymmetry of the source and drain ends of the crystal.

The sign of the charge associated with a pulse can be either negative or positive as concluded from the comparison of the directions of the electric field and pulse propagation. We found that upon reversal of the current a source is either inoperational or emits pulses with a reversed charge.

The longest pulse width observed did not exceed 5 ms at 77 K but could be significantly shorter depending on the sample. Figure 10(d) shows narrow peaks forming 1.4-kHz oscillations with constant phase shifts between segments on sample *KL*. On a given sample both the pulse width and the time delay between segments increase as the temperature decreases. In different crystals pulses of similar widths propagate with different delays even if the repetition frequency is the same. No evident relation between segment lengths and pulse widths or delays has been found. The delay, however, has never exceeded the pulse width. Together with the width, the charge associated with the pulses varies in a wide range. It seems that pulses carrying an arbitrarily small charge may exist, but there is an upper bound of the charge magnitude. This maximum charge was in the order of $2e$ per conducting chain.

In summary, the pulses observed on sample *RBL* and characterized in detail in the first part of this section are stable in the sense that they travel along the whole length of the crystal, and they originate from the same source. In some other cases the situation may be more complicated: several sources may operate simultaneously, the spatial range of the pulses may be restricted, etc. However, voltage pulses propagating along the crystal have been observed on all samples investigated.

C. Distinction of source and drain by combined ac and dc fields

In Sec. II B we concluded that the pulses are created at well-defined sources within the crystal. The observation that on the τ versus $1/f$ plot τ saturates at low repetition frequencies suggests that different factors control the pulse creation and pulse propagation. In the following we attempt to investigate the pulse creation and pulse propagation separately. We have performed experiments where the current in the segment in which the pulses are created is different from the current in the rest of the sample. In a complementary experiment the current is

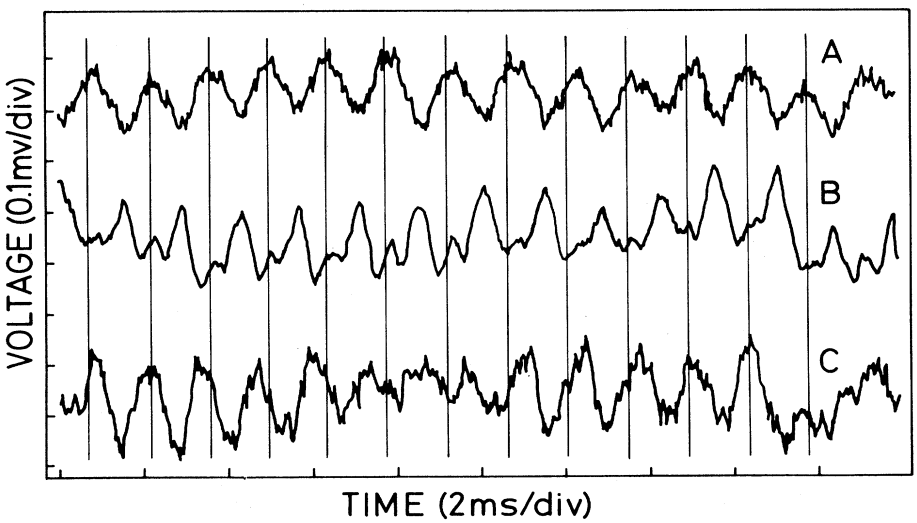

FIG. 10. Narrow pulses on sample *KL* forming high-frequency oscillations. The time delay between different segments shows up as a phase shift of the oscillations. The vertical lines are guides to the eye. The spacing of the lines is equal to the period of the oscillations.

homogeneous along the sample, but we suddenly decrease the current *during* the pulse to see if propagation can take place in a field lower than threshold once the pulse is created.

In the first kind of experiments we make use of the effect of mode locking,[6,13] i.e., the interference between the internal pulse creation frequency and an external ac drive. In Fig. 11 we demonstrate that the quasiperiodic voltage pulses can be synchronized by an external ac current superimposed on a dc bias. Figure 11(a) shows a sequence of pulses and its Fourier spectrum for a dc current without applying an ac drive. The spectrum is broad and structureless. Figure 11(b) shows the response to a combined ac and dc current both in time and frequency domains. The frequency of the ac signal is 45 Hz, about half the repetition rate in the dc case. Mode locking occurs for small applied ac fields, the amplitude of the external ac signal is comparable to the amplitude of the voltage pulse generated within the sample. The mode locking is obvious in both representations. In the time domain the relative phase of the external ac signal and the voltage pulses is constant. In the frequency domain the whole spectral weight is in narrow peaks at the external frequency and its harmonics. The harmonic generation is much larger than expected from the nonlinearity of I-V characteristics.

The next step is to apply the external alternating current to one segment only while the dc current flows through all three segments as shown in Fig. 12(a). We have determined by dc time-delay measurements the direction of pulse propagation. We denote by A and C the segments in which the pulse source and drain are located, respectively. Figure 12(b) shows the pulse frequency as a function of the external drive frequency at a con-

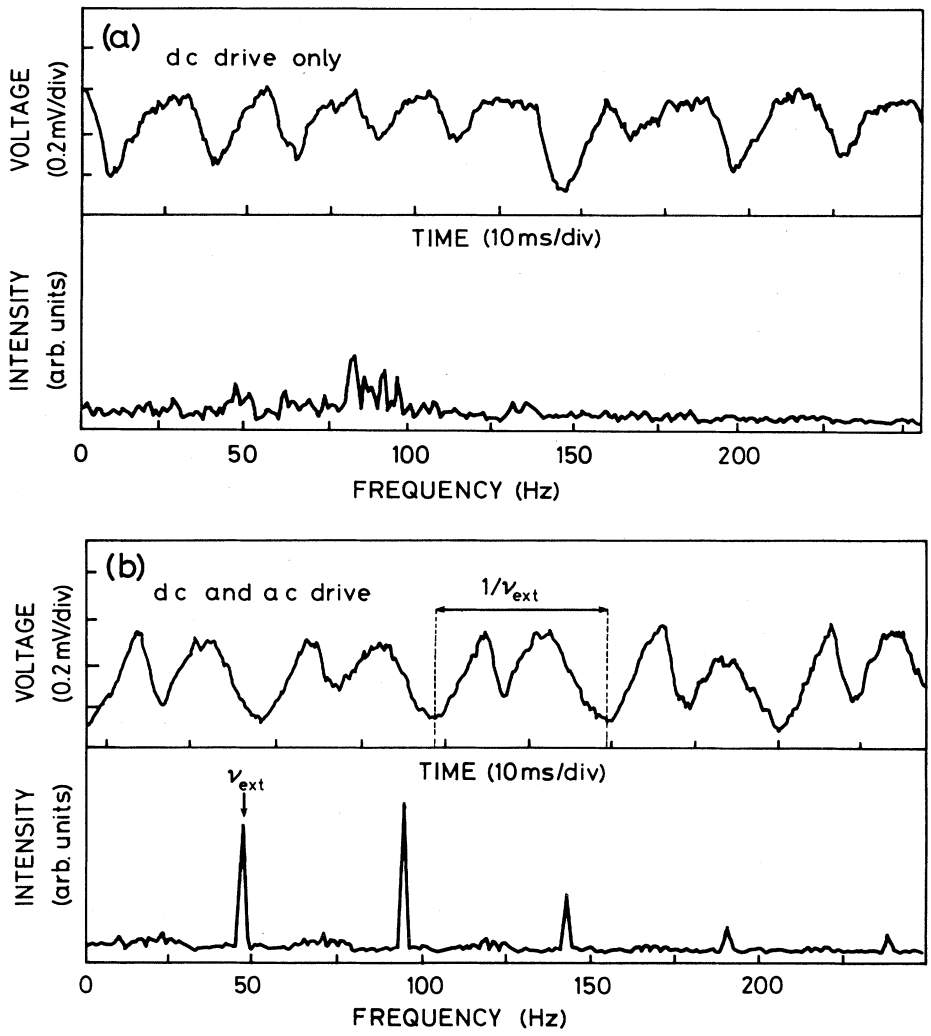

FIG. 11. Mode locking of the voltage pulses by an external sinusoidal ac drive. (a) A sequence of pulses and its Fourier spectrum for a dc current only without any external ac drive. (b) The time and frequency domain representations of the voltage response to a combined ac and dc drive. The frequency of the external drive, ν_{ext}, and its period, $1/\nu_{ext}$, are indicated in the figure. The internal pulse creation frequency is two times ν_{ext} (sample RBL, $T=77$ K).

stant dc bias in two different configurations. In one configuration the ac drive is applied to the source (A), and the pulses are detected on the drain (C). At low external frequencies ν_{ext}, the pulse creation frequency ν is larger than ν_{ext}. As ν_{ext} increases, the pulse frequency locks to it and remains locked over a wide range of frequencies until ν unlocks again at high ν_{ext}. In the reversed configuration where ν_{ext} is applied to the drain and the pulses are detected at the source, no locking occurs, and ν stays constant in the whole frequency range; no anomaly is observed when ν_{ext} crosses ν.

Another representation of the same phenomenon is shown in Fig. 13. In this case ν_{ext} is kept constant and the pulse creation frequency is measured as a function of the dc bias. As a reference, we also show the curve measured without an ac drive. When the locking signal is on the source, mode locking appears as a plateau at ν_{ext} on the ν versus I_{dc} curve. At the same time the curve is shifted towards lower currents with respect to the curve without an ac drive due to the nonlinear dependence of the pulse creation frequency on the total current. In the reversed configuration (ac drive on the drain) the curve is identical with the reference, i.e., no mode locking or shift occurs. The spectacular asymmetry of the source and drain segments in these experiments indicates that pulse creation in the source segment is independent to a high extent of the electric field on the segment far from the source.

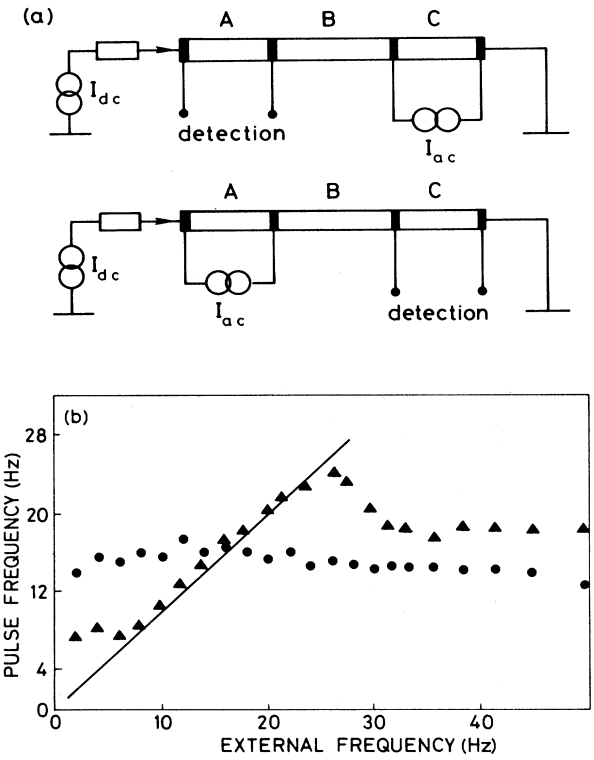

FIG. 12. Mode locking with external ac drive applied to one of the segments only (sample KM, $T=77$ K). (a) The two configurations used in this experiment. In addition to the dc current flowing through the sample an ac current source is connected to the segment at the end of the sample. The pulses are detected by the oscilloscope connected to the segment far from the ac drive. In the two configurations the ac drive and the oscilloscope are exchanged. (b) The internal pulse creation frequency as a function of the external ac drive frequency in the two configurations depicted in (a). Triangles, the ac drive is on segment A where the voltage pulses are created (source); circles, the ac drive is on segment C where the pulses are annihilated (drain). The location of the pulse creation has been determined by an independent dc time-delay measurement. The solid lines is $\nu=\nu_{ext}$. Frequency pulling is only seen when the ac drive is on the source segment. The dc current was $I_{dc}=365$ μA, the ac amplitude was 60 μA.

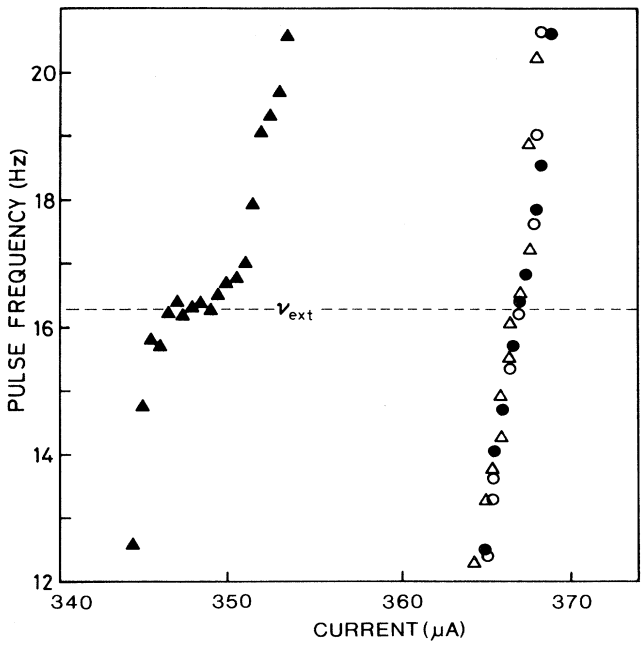

FIG. 13. The internal pulse creation frequency as a function of dc current in the same two configurations as in Fig. 12. Solid triangles, ac drive on the source; solid circles, ac drive on the drain. ν_{ext} is constant (dashed line). ν measured *without* external ac drive is also indicated (open circles and triangles, respectively). The pulse creation frequency is only affected if the ac drive is on the source. The plateau is due to the mode locking, the shift of the curve towards low currents is due to the nonlinear dependence of the pulse creation frequency on the total current (sample KM, $T=77$ K).

D. Propagation in fields below threshold

We have performed various experiments to investigate the possibility of pulse propagation in electric fields lower than the nonlinear threshold. In a typical experiment the current (homogeneous through the sample) is switched periodically between two levels: I_{hi} above threshold and I_{lo} below threshold (Fig. 14). I_{hi} is applied for time T_{hi} then I_{lo} is applied for time T_{lo}. With T_{hi} long enough, a pulse appears with a delay after the rising edge of the current (locked to the edge) as shown in Fig. 14(a). After

the mode locking is established, T_{hi} is appropriately reduced so that the current is decreased below threshold during the pulse [Fig. 14(b)]. We observe that in this case the pulse continues to propagate although the pulse amplitude and thus the charge carried by the pulse is smaller.

In a similar experiment, not detailed here, the current was constant in time but different in the source segment and other parts of the sample. We were able to detect pulses in segment C even if the current was below threshold in B and C provided the current was above threshold in segment A where the source was located.

III. DISCUSSION

The first question to address is the nature of the charge carriers that lead to the conductivity enhancement during the pulses. We propose that the extra charge is carried by moving CDW phase dislocation loops envisioned by Lee and Rice.[39] The majority of our results can be coherently explained within this picture.

Several experiments[15,34] suggest that for fields close to the threshold the CDW is depinned in part of the crystals only. Apart perhaps from samples of extremely good quality the CDW current is inhomogeneous even for fields well above threshold where NMR motional narrowing[15] shows that practically all the crystal is in the depinned state. The reason for inhomogeneous depinning may be the inhomogeneous distribution of pinning centers, particularly macroscopic defects such as inclusions, and inhomogeneous current injection determined by the particular geometry of electrode contacts. Crystal surfaces may also play a role.[41,42] On the other hand, model calculations[34,36] suggest and x-ray diffraction measurements[43] demonstrate that the CDW phase coherence length is long in all directions even in

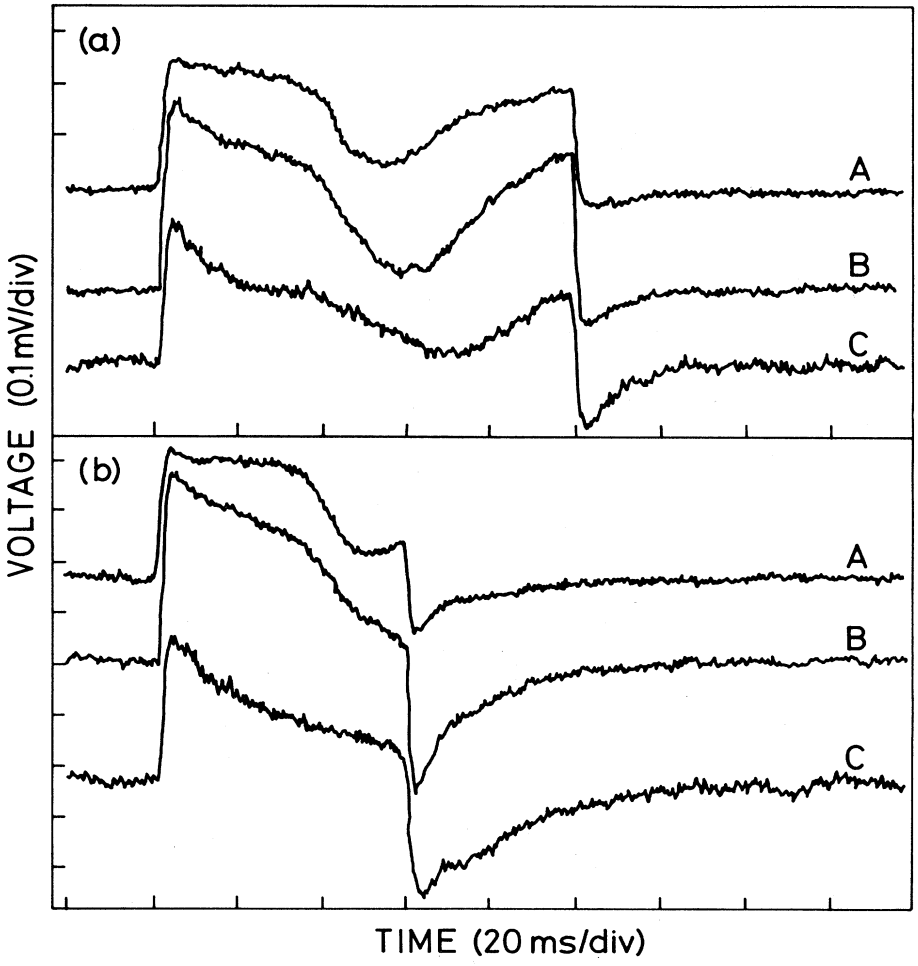

FIG. 14. Pulse propagation in a field below threshold (sample *RBL*, $T=77$ K). The current is switched periodically from a current $I_{lo}=71$ μA below threshold to a current $I_{hi}=74$ μA above threshold. After an interval T_{hi} the current is switched back to I_{lo}. Time-delayed pulses appear in all three segments while the current is high. (a) If T_{hi} is long enough the pulse propagation terminates before the current is switched to the low value. (b) T_{hi} is short and the current is switched to I_{lo} *during* pulse propagation. The pulse continues to propagate although the current is smaller than that required for pulse creation (sample *RBL*, $T=77$ K).

the sliding state. Consequently, the solution of the boundary problem arising on the surfaces between regions of moving and pinned CDW is very unlikely to be a misfit of the CDW phase on the whole surface, rather it is the motion of the CDW phase dislocations along the surface.

Since the displacement field of CDW phase deformations is uniaxial, the Burgers vector of a CDW dislocation is also uniaxial and parallel to the conducting chains. Let us consider an edge dislocation loop lying in a plane perpendicular to the chains. Such a loop fulfills two important requirements for the charge carriers giving rise to the pulse propagation phenomenon. First, each chain within the dislocation loop contains an extra charge of $2e$ (or $-2e$) compared to th chains outside the loop, so the total charge of the loop can be macroscopic as observed for the pulses. Second, the extra charge is localized to the plane of the dislocation loop, and if the loop glides along the chains, the motion of localized charges may result in time-delayed pulses on different segments.

A possible mechanism for the creation of dislocation loops is the Frank-Read mechanism as analyzed by Lee and Rice.[39] Other thermal[30] and athermal[33] mechanisms have also been proposed. In any case, strong pinning centers are expected to play an important role in the nucleation process, which may be the explanation of our observation that pulse creation is localized within the crystal.

There are some important differences[33] between the motion of CDW dislocations and dislocations in crystal lattices. In addition to the shear stress as the driving force of the motion parallel to the Burgers vector of dislocations ("gliding"), CDW dislocation loops are subject to a surface force due to the interaction of the excess charge within the loop with the electric field. The motion of dislocations perpendicular to the chains and to the Burgers vector ("climbing") is driven by the elastic stress of the CDW superlattice. Since climbing does not conserve mass, in crystals it is slow because it requires the migration of vacancies or interstitials. In CDW's climbing is made possible by conversion between the normal electron and CDW electron fluids. In fact, Ong, Verma, and Maki[19] proposed that the most effective mechanism for CDW–normal-electron conversion (which must occur at least in the vicinity of electrode contacts for a stationary CDW current to flow) is the transverse motion of CDW dislocations. On the other hand gliding conserves the CDW charge.

The above difference between longitudinal and transverse dislocation motions explains that different factors control the creation and the propagation of the pulses. This is seen in many experiments: The propagation delay (or velocity) remains finite as the generation frequency tends to zero with the electric field approaching the generation threshold. With decreasing temperature the threshold field for generating pulses decreases, but the propagation delay and linewidth increases indicating a larger damping of the gliding motion. The most spectacular of this kind of experiment is the pulsed current measurement where after creation the pulse can propagate even in a field below threshold. The threshold corresponds to the creation but not to the propagation of pulses.

The total charge carried by an edge dislocation loop is $\pm 2en_{\perp}S$ where S is the surface area bounded by the loop and $n_{\perp}$ is the number of chains crossing unit surface. The sign can be either positive or negative allowing pulse propagation parallel or antiparallel to the field in accordance with experiment. The measured maximum charge is consistent with maximum loop surfaces close to the sample cross-sectional area on several samples and in a wide range of temperature and field.

In this picture the distribution of charge magnitudes (Fig. 6) reflects the distribution of the surface, S, spanned by the loop. Even when broad, this distribution is structureless, and no sign of charge quantization is found as expected for dislocations of continuously varying size. This is in contrast to the amplitude quantization[12] of aperiodic voltage steps observed in TaS_3. The decrease of charge carried by a pulse upon decreasing the field below threshold after the pulse is created is understood in the model as the shrinking of its surface.

Even if the charge associated with the pulses indicates a loop surface close to the sample cross section, only a small fraction (below 10% in sample *RBL*) of the nonlinear current is contained in the large pulses investigated. The assumption that all the nonlinear current is carried by dislocation loops requires the simultaneous existence of smaller loops giving rise to a background noise. The paths of dislocation loops may overlap.

The experimentally measured charge may have a contribution from changes of the conductivity by normal electrons. In fact the very long-time tail of the pulses can hardly be interpreted as the motion of localized CDW charge. Such an interpretation would require the motion of charges in the order of 10^2e per chain by a velocity in the order of 10^{-5} m/s (the latter estimated from the pulse width and segment length). Rather, the time scale (a few tens of seconds) is suggestive of normal resistance relaxation[44] due to the slow rearrangement of the CDW phase distribution following the passage of the pulse. A model for the contribution of phase defects to the normal resistance has been proposed by Maki.[30] In addition to the different time scales the separation of the propagating pulse from the long tail is justified by the observation that the sign of the long tail can be either positive or negative. This observation is consistent with the interpretation that the origin of the tail is normal resistance relaxation since it can lead to both an increase and decrease of the resistance. On the other hand the propagating pulses always appear as a conductivity enhancement. The charge integral in Eq. (2) is insensitive to the upper bound in the range of a few times the pulse width at half maximum suggesting that the contribution of the process leading to the tail is small at short times compared to that of the propagating pulse.

The propagation velocity, v, inferred from the propagation delay is in the order of 1 m/s. This is about 3 orders of magnitude smaller than the phason velocity.[45] In a simplified picture the pulse width is $W=(d+l)/v$ where l is the segment length and d is the longitudinal extent of the charge carrier, while the delay is $\tau=l/v$. This is in

agreement with the finding that W and τ increase with the same rate as the temperature decreases provided d is constant or at least its change is not as fast as the exponential decrease of the other two quantities.

The observation that $W \gtrsim \tau$ implies that the spatial extent of the carriers is in the order of the sample length indicating that pulse propagation is more complex than the motion of a charge localized in the plane of a dislocation loop. A possible explanation is that long-range CDW deformations form during pulse creation. The relaxation of the CDW deformations on the millisecond scale[46] may then influence the pulse shapes and complicate the experimental determination of propagation delay. The behavior at high generation frequencies reflects the long-range interaction of successive pulses. We have never observed two pulses in the same segment, i.e., the propagation delay was always shorter than the time delay between successive pulses on the same segment. This suggests that the perturbation of the field and elastic stress by an emitted pulse influences the formation of the succeeding one. On the other hand, the spectacular asymmetry of the "source" and "drain" segments in the mode-locking experiments unambiguously show that pulse creation is localized within the sample and highly independent of the electric field in the segment far from the one where the pulse is created.

In the following we examine the possibility that the narrow-band noise observed in all CDW systems has the same origin as the voltage pulses studied in this paper. Obviously, the voltage pulses possess most of the distinguishing properties of NBN. The pulse generation rate increases with increasing electric field and at high repetition rates the pulses form oscillations with fairly high coherence. Although it is difficult to prove it directly, the charge carried by the pulses is consistent with $2e$ per chain in accordance with Eq. (1). Like NBN, the voltage pulses display interference phenomena in combined ac and dc fields.

The most serious difficulty of identifying the NBN and voltage pulse phenomena is the frequency range of observability. While NBN has been observed up to several hundred kHz in blue bronzes[34] and up to several hundred MHz in $NbSe_3$,[7] the highest well-defined frequency we have found is about 2 kHz. We continue our search for samples with coherent high-frequency oscillation. Preliminary results on TaS_3 indicate the existence of coherent, time-delayed oscillations on different sample segments up to 100 kHz.

In conclusion, we have described a voltage instability related to the depinning of CDW's in the blue bronzes $K_{0.3}MoO_3$ and $Rb_{0.3}MoO_3$. Voltage pulses are created at well-defined locations within the crystal and appear with a time delay in other segments of the sample. The maximum charge displaced by a voltage pulse is in the order of $2e$ times the number of conducting chains in the crystal. The pulse generation frequency increases and the time delay decreases with increasing electric field. Pulse propagation shows an exponential slowing down with decreasing temperature. We interpret the voltage instability in the framework of a moving CDW dislocation model proposed by Lee and Rice.[39] The low velocity propagation may be crucial in the understanding of the narrow-band noise.

ACKNOWLEDGMENTS

We are indebted to K. Kamaras, B. Keszei, and J. Marcus for preparing the samples. This research was supported by the Hungarian National Scientific Research Fund (OTKA) under Contract No. 1787 and by the Hungarian Academy of Sciences under Contract No. AKA 86-292.

[1]For recent reviews on CDW conduction see G. Grüner, Rev. Mod. Phys. **60**, 1129 (1988); *Low Dimensional Conductors and Superconductors,* edited by D. Jérome and L. G. Caron (Plenum, New York, 1987).

[2]P. Monceau, N. P. Ong, A. M. Portis, A. Meerchaut, and J. Rouxel, Phys. Rev. Lett. **37**, 602 (1976).

[3]John Bardeen, Lect. Notes in Phys. **95**, 3 (1979); in *Highly Conducting One-Dimensional Solids,* edited by J. T. Devreese, R. P. Evrand, and V. E. Van Doren (Plenum, London, 1979), p. 373.

[4]H. Fröhlich, Proc. R. Soc. London, Ser. A **223**, 296 (1954).

[5]R. M. Fleming and C. C. Grimes, Phys. Rev. Lett. **42**, 1423 (1979).

[6]For a review on noise and interference phenomena in CDW systems see G. Grüner (unpublished).

[7]R. E. Thorne, J. R. Tucker, and John Bardeen, Phys. Rev. Lett. **58**, 828 (1987); R. E. Thorne, W. G. Lyons, J. W. Lyding, and J. R. Tucker, Phys. Rev. B **35**, 6348 (1987).

[8]J. Richard, P. Monceau, M. Papoular, and M. Renard, J. Phys. (Paris) Colloq. **15**, C-7157 (1982); A. Zettl and G. Grüner, Solid State Commun. **46**, 29 (1983); A. Maeda, M. Naito, and S. Tanaka, J. Phys. Soc. Jpn. **54**, 1912 (1985).

[9]A. Zettl and G. Grüner, Phys. Rev. B **26**, 2298 (1982).

[10]J. C. Gill and A. W. Higgs, Solid State Commun. **48**, 709 (1983).

[11]J. Dumas, C. Schlenker, J. Marcus, and R. Buder, Phys. Rev. Lett. **50**, 757 (1983); J. Dumas, A. Arbaoui, H. Guyot, J. Marcus, and C. Schlenker, Phys. Rev. B **30**, 2249 (1984).

[12]N. P. Ong, C. B. Kalem, and J. C. Eckert, Phys. Rev. B **30**, 2902 (1984).

[13]P. Monceau, J. Richard, and M. Renard, Phys. Rev. Lett. **45**, 43 (1980).

[14]See, e.g., John Bardeen, E. Ben-Jacob, A. Zettl, and G. Grüner, Phys. Rev. Lett. **49**, 493 (1982).

[15]A. Jánossy, C. Berthier, P. Ségransan, and P. Butaud, Phys. Rev. Lett. **59**, 2349 (1987).

[16]S. E. Brown and G. Grüner, Phys. Rev. B **31**, 8302 (1985).

[17]Yu. I. Latyshev, V. E. Minakova, and Ya. A. Zhanov, Pis'ma Zh. Eksp. Teor. Fiz. **46**, 31 (1987).

[18]G. Grüner, A. Zawadowski, and P. Chaikin, Phys. Rev. Lett. **46**, 511 (1981).

[19]L. M. Sneddon, M. C. Cross, and D. S. Fisher, Phys. Rev. Lett. **49**, 292 (1982).

[20]N. P. Ong, G. Verma, and K. Maki, Phys. Rev. Lett. **52**, 663

(1984).
[21]N. P. Ong and K. Maki, Phys. Rev. B **32**, 6582 (1985).
[22]L. P. Gor'kov, Pis'ma Zh. Eksp. Teor. Fiz. **38**, 76 (1983) [JETP Lett. **38**, 87 (1983)]; Zh. Eksp. Teor. Fiz. **86**, 1818 (1984).
[23]G. Mozurkewich and G. Grüner, Phys. Rev. Lett. **51**, 2206 (1983); G. Mozurkewich, M. Maki, and G. Grüner, Solid State Commun. **48**, 453 (1983).
[24]S. E. Brown and L. Mihály, Phys. Rev. Lett. **55**, 742 (1985).
[25]T. W. Jing and N. P. Ong, Phys. Rev. B **33**, 5841 (1986).
[26]A. Zettl, M. B. Kaiser, and G. Grüner, Solid State Commun. **53**, 649 (1985).
[27]G. Verma and N. P. Ong, Phys. Rev. B **30**, 2928 (1984).
[28]S. E. Brown, A. Jánossy, and G. Grüner, Phys. Rev. B **31**, 6869 (1985).
[29]J. W. Lyding, J. S. Hubacek, G. Gammie, and R. E. Thorne, Phys. Rev. B **33**, 4341 (1986).
[30]K. Maki, Physica B+C **143**B, 59 (1986); Kazumi Maki and Xiao Zhou Huang, Phys. Rev. B **37**, 8668 (1988).
[31]J. R. Tucker, W. G. Lyons, and G. Gammie, Phys. Rev. B **38**, 1148 (1988); J. R. Tucker and W. G. Lyons, *ibid.* **38**, 7854 (1988).
[32]J.Dumas and D. Feinberg, Europhys. Lett. **2**, 555 (1986).
[33]D. Feinberg and J. Friedel, J. Phys. (Paris) **49**, 485 (1988).
[34]See, e.g., A. Jánossy, G. Kriza, S. Pekker, and K. Kamarás, Europhys. Lett. **3**, 1027 (1987).
[35]J. C. Gill, Solid State Commun. **44**, 1041 (1982).
[36]G. Mihály, Gy. Hutiray, and L. Mihály, Phys. Rev. B **28**, 4896 (1983).
[37]M. C. Saint-Lager, P. Monceau, and M. Renard, Europhys. Lett. **9**, 585 (1989).
[38]T. Csiba, G. Kriza, and A. Jánossy, Europhys. Lett. **9**, 163 (1989).
[39]P. A. Lee and T. M. Rice, Phys. Rev. B **19**, 3970 (1979).
[40]For reviews see C. Schlenker and J. Dumas, in *Crystal Chemistry and Properties of Materials with Quasi-One-Dimensional Structures,* edited by J. Rouxel (Reidel, Dordecht, 1986), p. 135; C. Schlenker, in *Quasi-One-Dimensional Conductors and Superconductors* (Plenum, New York, 1987), p. 477.
[41]D. V. Borodin, F. Ya. Nad', Y. S. Savitskaya, and S. V. Zaitsev-Zotov, Physica B+C **143B**, 73 (1986).
[42]J. C. Gill, Physica B+C **143B**, 49 (1986).
[43]R. M. Fleming, R. G. Dunn, and L. F. Schneemeyer, Phys. Rev. B **31**, 4099 (1985).
[44]L. Mihály, Ting Chen, B. Alavi, and G. Grüner, in *Charge-Density Waves in Solids,* Vol. 219 of *Lecture Notes in Physics,* edited by Gy. Hutiray and J. Sólyom (Springer, Berlin, 1985), p. 455.
[45]J. P. Pouget, S. Girault, A. H. Moudden, B. Hennion, C. Escribe-Filippini, and M. Sato, Phys. Scr. **T25**, 58 (1989).
[46]G. Kriza and G. Mihály, Phys. Rev. Lett. **56**, 2529 (1986).